

**BaCe_{0.25}Mn_{0.75}O_{3-δ} — A promising perovskite-type oxide for solar thermochemical hydrogen production**

Journal:	<i>Energy & Environmental Science</i>
Manuscript ID	EE-ART-07-2018-001989.R1
Article Type:	Paper
Date Submitted by the Author:	16-Aug-2018
Complete List of Authors:	Romero Barcellos, Debora; Colorado School of Mines, Department of Metallurgical and Materials Engineering Sanders, Michael; Colorado School of Mines, MME Tong, Jianhua; Clemson University, Materials Science and Engineering; Clemson University, Materials Science and Engineering McDaniel, Anthony H.; Sandia Labs, O'Hayre, Ryan; Colorado School of Mines, Dept of Metallurgical and Materials Engineering

$\text{BaCe}_{0.25}\text{Mn}_{0.75}\text{O}_{3-\delta}$ — A promising perovskite-type oxide for solar thermochemical hydrogen production

Debora R. Barcellos, Michael Sanders, Jianhua Tong[□], Anthony H. McDaniel[□], Ryan O'Hayre

Colorado School of Mines, Department of Metallurgical and Materials Engineering, Golden, CO, USA

[□]Clemson University, Clemson, Materials Science and Engineering, SC, USA

[□]Sandia National Laboratories, Combustion Research Facility, Livermore, CA, USA

ABSTRACT

Solar-thermal based hydrogen production technologies employing two-step metal oxide water-splitting cycles are emerging as a viable approach to renewable and sustainable solar fuels. However, materials innovations that overcome thermodynamic constraints native to the current class of solar-thermal water splitting oxides are required to increase solar utilization and process efficiency. Lowering oxide thermal reduction temperature while maintaining high water-splitting favorability are important ways to enhance such performance metrics. Recent attention to perovskite-type oxides as an alternative to ceria, which is widely viewed as the state-of-the art redox material, is driven by demonstrated thermodynamic and structural tuning derived through engineered composition. Here we discuss the unique properties of $\text{BaCe}_{0.25}\text{Mn}_{0.75}\text{O}_3$ (BCM) within the context of thermochemical water splitting materials. Firstly, BCM is a novel example of a line compound with B-site substitution of Mn by Ce. It also exhibits a polymorph phase transition during thermal reduction and yields nearly 3× more H_2 than ceria when reduced at lower temperature (1350 °C). More importantly, BCM exhibits faster oxidation kinetics and higher water-splitting favorability than $\text{Sr}_x\text{La}_{1-x}\text{Mn}_y\text{Al}_{1-y}\text{O}_3$ ($x, y = 0.4, 0.6$), which is a well-studied and popular Mn-based perovskite formulation. The unique properties manifested by BCM through engineered composition offer new pathways towards unlocking higher performing materials for solar thermochemical water splitting.

INTRODUCTION

A solar-driven two-step thermochemical cycle for splitting either water (so called STCH or STC hydrogen) or carbon dioxide utilizing metal oxides has the potential to provide industrial-scale quantities of renewable solar fuels. First proposed by Nakamura,¹ the cycle chemistry is deceptively simple and avoids known technological barriers associated with other multistep gas-splitting cycles.^{2,3} Unfortunately even the simple stoichiometric cycle chemistries proposed by Nakamura and others are subject to undesired thermally-driven phenomena, such as phase change, metal volatilization, sintering, and complex solid solution behavior, that have thus far confounded further development of the approach.^{4,5} Recently, non-stoichiometric oxides have emerged as the preferred redox-active material for two-step gas-splitting cycles because they are able to maintain phase stability under the extreme thermal and chemical stresses encountered in a solar thermochemical reactor environment.⁶ In this approach, a suitable oxide is defected by driving oxygen spontaneously from the lattice at high temperature. However, unlike the stoichiometric reaction, the oxygen deficiency does not result in phase change, decomposition, or disproportionation. When the reduced oxide is exposed to steam or carbon dioxide at conditions suitable for spontaneous reoxidation, oxygen is stripped from the gas molecule and transferred back into the oxide. And as in the stoichiometric cycle, hydrogen or carbon monoxide is the net product of the reactions.

Ceria (CeO_2) remains the benchmark material for single-phase non-stoichiometric STCH cycling.⁶ It is favored because of a combination of phase stability, fast redox kinetics, and high fuel selectivity.^{7,8} One of ceria's greatest attributes is high tolerance to the presence of hydrogen during reoxidation. Ceria will thermodynamically favor net hydrogen production over deeper metal oxide reduction when splitting water under exceedingly low gas-phase oxygen chemical potential (i.e., at high fuel selectivity and low steam-to-hydrogen ratio; $\sim 2:1$ ⁹). This attribute results in reasonable fuel selectivity for reoxidation conditions with gas-phase oxygen chemical potential many orders of magnitude below that of the thermal reduction condition. Unfortunately, these benefits are offset by the extremely high temperature (>1550 °C) required to reduce ceria to an extent deemed commercially viable.^{10,11} The combination of complicated engineering, exotic materials, and greatly reduced solar receiver efficiencies necessary to support such temperatures make the need for reduction temperatures below 1400 °C imperative.^{12,13} Efforts to overcome ceria's thermal reduction limitation have largely failed,¹⁴⁻¹⁹ thus necessitating a search for new redox materials that can sustain both high fuel selectivity and high fuel yield, but at lower thermal reduction temperatures.

Increasingly, the search for new STCH cycle materials has turned towards perovskite-structured oxides.²⁰ Perovskites have many desirable traits, including high structural tolerance for non-

stoichiometry, tunable point-defect thermodynamics, good chemical stability and a long history of application in related fields that require oxygen exchange functionality (such as solid oxide fuel cells,²¹ chemical looping,²² and electrochemical water splitting²³). While research into perovskite-based STCH materials is still in its infancy, several compounds including $\text{Sr}_x\text{La}_{1-x}\text{Mn}_y\text{Al}_{1-y}\text{O}_{3-\delta}$ (SLMA)²⁴ and $\text{La}_{0.6}\text{Ca}_{0.4}\text{Mn}_{1-y}\text{Al}_y\text{O}_{3-\delta}$ (LCMA)²⁵ have shown promise.

Based on the insights provided by these prior perovskite oxide candidates, we identified the $\text{BaCe}_x\text{Mn}_{1-x}\text{O}_{3-\delta}$ perovskite as a potential source of new STCH materials. Our selection of this system is based on leveraging the desired perovskite-associated traits mentioned above, particularly the ability to tune the point defect thermodynamics. Here this is achieved by double occupancy of the B-site using both cerium and manganese cations. We hypothesize that the multi-valent transition metal Mn cation will act in the accommodation of charge accumulation during redox (likely as $\text{Mn}^{4+}/\text{Mn}^{3+}$) while the Ce-Mn site mixing will allow for optimization of the oxygen vacancy formation energy. As shown in Table 1, the estimated oxygen vacancy formation energy (E_v) for BaMnO_3 is extremely low (near zero) while E_v for BaCeO_3 is extremely high (near 20 eV). Although sufficient experimental data is not available to satisfactorily establish E_v with high confidence in these compounds, alternative measures for E_v (e.g., based on a recent simple formula for estimating E_v in oxides developed by Deml et al.²⁶) or comparisons of the bond dissociation energies for Mn-O and Ce-O bonds show the same trends: BaMnO_3 is easy to reduce as the Mn-O bond is relatively weak, while BaCeO_3 is difficult to reduce because the Ce-O bond is relatively strong. Thus, Mn/Ce B-site mixing in the $\text{BaCe}_x\text{Mn}_{1-x}\text{O}_{3-\delta}$ system may provide a pathway to optimize E_v between these two extremes. Furthermore, this strategy enables thriftiness of the expensive rare-earth element Ce in a STCH-active compound while still retaining its beneficial properties. Ceria has long been understood to yield beneficial thermodynamics based on its rare increase in entropy during reduction over the range of defect concentrations in the fluorite phase relevant to STC. This has been recently shown to be related directly to cerium's electronic structure,^{27,28} and leads to the possibility of cerium additions to other systems having positive entropic impacts.

In this paper, we explore the water splitting efficacy of $\text{BaCe}_x\text{Mn}_{1-x}\text{O}_{3-\delta}$ and compare the redox activity of this material system against a CeO_2 benchmark and SLMA. Of particular interest here, and unique to this effort, is our exploration of the extent to which $\text{BaCe}_x\text{Mn}_{1-x}\text{O}_{3-\delta}$ maintains water splitting favorability under reoxidation conditions that are challenged by low gas-phase oxygen chemical potential (e.g., $\text{H}_2\text{O}:\text{H}_2$ ratio <2000). Such water splitting conditions are rarely investigated by this research community, yet considered a key metric when screening for commercial viability.^{9,29}

Table 1 – Oxygen vacancy formation energies and oxygen-cation bond dissociation energies for the two family end-member compounds (BaMnO₃ and BaCeO₃). See supplemental information for details on the calculation of E_v based on Deml's model.

Compound	E_v reported in the literature (eV)	E_v calculated based on Deml's model (eV) ²⁶	Bond dissociation energy Ce-O or Mn-O (eV) ³⁰
BaMnO ₃	0.04 ³¹	4.1	3.75
BaCeO ₃	19.20 ³²	15.1	8.19

EXPERIMENTAL

Initially, seven different compound formulations were synthesized to test the redox behavior of a large breadth of the BaCe_xMn_{1-x}O_{3-δ} compositional range: $x = 0, 0.05, 0.15, 0.25, 0.50, 0.75,$ and 1, which we label BMO, BC05M95, BC15M85, BC25M75, BC50M50, BC75M25, and BCO respectively. All seven compositions were synthesized using a sol-gel modified Pechini method.³³ In brief, stoichiometric amounts of the precursors, barium nitrate (Alfa Aesar 99 %), cerium nitrate (Alfa Aesar 99.5 %) and manganese acetate tetrahydrate (Alfa Aesar 98 %) were dissolved in deionized water and constantly stirred with ethylenediaminetetraacetic acid (EDTA) and citric acid under heat. Ammonium hydroxide was used to adjust the pH. Once the gels were formed, they were dried at 165 °C and subsequently calcined using a two-step heat-treatment profile designed to avoid Mn loss; first, the powders were calcined at 800 °C for 10 h at a ramp rate of 10 °C/min and cooled back to 75 °C; then the powders were calcined at the final temperature of 1400 °C for 5 h at the same heating rate. Later, pure phase BaCe_{0.25}Mn_{0.75}O_{3-δ} was produced using the same technique.

Sr_{0.4}La_{0.6}Mn_{0.6}Al_{0.4}O_{3-δ} (SLMA4664) and Sr_{0.6}La_{0.4}Mn_{0.6}Al_{0.4}O_{3-δ} (SLMA6464) were synthesized following a similar approach. Strontium nitrate, aluminum nitrate, manganese nitrate tetrahydrate, and lanthanum nitrate hexahydrate were dissolved in deionized water and added to ammonium hydroxide, EDTA and citric acid heated at 80-120 °C until a gel formed. The gel was transferred to a drying oven at 250 °C for 3 h. The sample was crushed and calcined at 800 °C for 6 h. A second calcination was done at 1350 °C for 24 h. Commercial cerium oxide powder (Sigma Aldrich 99.995 %) was used for comparison.

Powder X-ray diffraction (XRD) was performed on all samples using a PANalytical PW3040 diffractometer in Bragg-Brentano geometry surveying the 2θ range between 20° and 120° at a step size of 0.008° and Cu Kα radiation of $\lambda = 1.540598$ and 1.54439 Å. PANalytical Highscore Plus software was used for Rietveld refinement.

High-temperature X-ray diffraction (HTXRD) was carried out at Sandia National Laboratories in Albuquerque at a Bragg-Brentano configuration XRD surveying the 2θ range between 19° and 50° with

CuK α radiation of $\lambda = 1.540598$ and 1.54439 \AA , using programmable divergence slit equipped with a Pt heating stage and controlled atmosphere. UHP He was used during the reduction step, flown through an oxygen getter which ensured a $p\text{O}_2$ of about 10^{-6} atm/atm.

The samples were prepared by firstly crushing them using a mortar and pestle and adding methanol to form a liquid solution. This solution was carefully deposited onto the (110) yttrium stabilized zirconia single crystal plate (10 x 10 x 0.5 mm) to obtain an even layer of sample. The XRD stage was rotated about 2° in the xz direction to avoid the YSZ single crystal diffraction peak during normal scan.

The HTXRD run was carried out by heating the sample at $10 \text{ }^\circ\text{C}/\text{min}$ from room temperature (RT) to $1350 \text{ }^\circ\text{C}$ in He flow taking a scan at every $50 \text{ }^\circ\text{C}$ from $850 \text{ }^\circ\text{C}$ to $1350 \text{ }^\circ\text{C}$ (each scan taking about 10 min to complete). The $1350 \text{ }^\circ\text{C}$ isotherm was held for 1h 30min.

Temperature Program Reduction (TPR) experiments were accomplished using a Setaram Setsys Evolution configured for thermal gravimetric analysis (TGA) with alumina crucibles to test the samples oxygen extent of reduction. The TPR experiment consisted of heating a sample at $10 \text{ }^\circ\text{C}/\text{min}$ to $1350 \text{ }^\circ\text{C}$ in UHP N_2 and holding isothermally for 1 h. The sample was subsequently cooled to $1000 \text{ }^\circ\text{C}$ followed by the introduction of air to initiate reoxidation. The change in mass was measured as a function of temperature and time.

The materials' water splitting capabilities were tested at Sandia National Laboratories in a stagnation flow reactor (SFR) coupled with a laser-based sample heater and a mass spectrometer downstream from the reactor. All systems were operated at sub ambient pressure (75 Torr), the details of which have been published elsewhere.³⁴⁻³⁶ The mass spectrometer was calibrated using aliquots of O_2 and H_2 prepared by mass flow controllers and taken from known gas mixture standards (25% O_2 in Ar and 5% H_2 in Ar). Powder samples ($\sim 100 \text{ mg}$) were placed on a zirconia platform forming a loosely-packed shallow bed, and the reactor was heated to the oxidation temperature (T_{OX}) under UHP Ar atmosphere. Samples were heated by the laser at $10 \text{ }^\circ\text{C}/\text{s}$ from T_{OX} to the reduction temperature (T_{RE}), where they were held for 330 s, unless indicated otherwise. Upon turning off the laser, the samples cooled to T_{OX} in a matter of seconds, minimizing the potential for reoxidation with any trace amount of O_2 still in the chamber. 40 vol.% water vapor (in Ar gas flow) was introduced to initiate reoxidation. The total amounts of O_2 released and H_2 produced were calculated by integrating the baseline-corrected mass spectrometer signals over the entire gas evolution envelope. A numerical approach developed by McDaniel et al.^{24,35,37} was used to extract pseudo second-order rate constants for H_2 production from the transient response function of the mass spectrometer. This procedure corrects the measured instrument response for physical phenomena such as gas mixing and detector time lag, which enables more accurate quantification of the materials' true solid-state kinetic response (see SI).

Finally, water splitting performance was tested under lower steam-to-hydrogen ratios to assess the material's performance under more realistic (i.e., "higher-conversion") WS conditions. Controlled amounts of hydrogen were mixed with steam, essentially fixing the initial gas-phase oxygen chemical potential prior to the reoxidation (WS) step. The steam-to-hydrogen ratios tested, with associated $\log(p_{O_2})$ values (in atm) at 850 °C, were 1333:1 (-11.6), 1000:1 (-11.9), 750:1 (-12.1), 500:1 (-12.5) and 285:1 (-13). In some instances, the controlled amounts of hydrogen introduced to the chamber generated a background hydrogen signal larger than the hydrogen produced by water splitting. Due to this background interference, the amount of hydrogen produced during the oxidation step was inferred from the oxygen peak measured during a subsequent reduction cycle. The material will only reduce in a subsequent cycle if it has oxidized in the previous cycle, ensuring validity of this indirect measurement approach. If no oxidation was achieved, then no subsequent reduction is detected in the following cycle.

RESULTS AND DISCUSSION

X-ray diffraction of all seven samples are reported in Figure S1. The identified phases, and their relative amounts as calculated by Rietveld refinement are shown in Figure 1. Analysis reveals that while the predicted mixed B-site occupancy occurs, all $BaCe_xMn_{1-x}O_{3-\delta}$ compositions besides the BCO and BMO end-members produce a perovskite-related line compound, $BaCe_{0.25}Mn_{0.75}O_{3-\delta}$, with the excess Ce and/or Mn accommodated by additional simple perovskite secondary phases such as $BaCeO_3$, $BaMnO_3$, as well as cerium oxide. Our observations of the $BaCe_xMn_{1-x}O_{3-\delta}$ phase behavior are consistent with Fuentes et al.³⁸, who concluded that the Ce/Mn B-site shared perovskite can only be formed in the 25% Ce/75% Mn ratio.

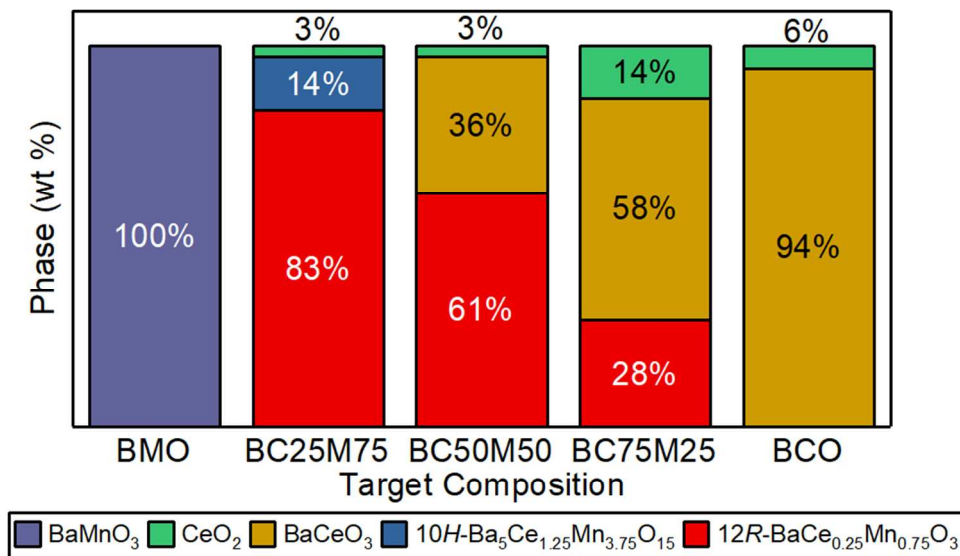


Figure 1 - Summary of phases present in five of the target compositions.

Interestingly, the $\text{BaCe}_{0.25}\text{Mn}_{0.75}\text{O}_{3-\delta}$ line compound exhibits two known polytypes: $12R$ and $10H$,^{39,40} with the $12R$ polytype generally believed to be the thermodynamically stable low-temperature phase. In our as-prepared samples, the $12R$ polytype dominates. Furthermore, Rietveld analysis of the BC25M75 sample before and after the first reduction/oxidation cycle indicates that the minority $10H$ polymorph phase converts almost completely to the $12R$ phase after the first cycle (see Table S2 and Figure S2). Thus, upon cycling, the BC25M75 sample attains >95% $12R$ - $\text{BaCe}_{0.25}\text{Mn}_{0.75}\text{O}_{3-\delta}$ phase purity, with only minor traces of $10H$ - $\text{Ba}_5\text{Ce}_{1.25}\text{Mn}_{3.75}\text{O}_{15-\delta}$ and CeO_2 .

To better understand the $12R$ to $10H$ behavior, HTXRD was performed at Sandia National Laboratories in Albuquerque. As Figure 2 demonstrates, under thermally reducing conditions the $12R$ phase slowly begins to convert to $10H$ upon heating above 1150°C . The oxygen non-stoichiometry appears to be required for this transition to occur, as HTXRD scans of $12R$ performed under air, do not show this phase transformation at 1150°C . With further heating under highly reducing conditions, the phase conversion behavior extends to a new, previously unreported, polytype H , that begins to appear around 1350°C and grows during the high temperature soak. This new phase requires even further non-stoichiometry to appear (the oxygen getter used on the HTXRD produces the required low oxygen partial pressure, only known to be below the 100 ppb sensitivity limit of the attached oxygen sensor) and also appears to be fully reversible. Initially, it was suspected that this phase was evidence of decomposition, however, we have successfully obtained nearly pure-phase H polytype after long high-temperature reductions and quenching. XRD analysis of this new polytype shows no evidence of additional phases (e.g. such as ceria or barium cerate) that would indicate decomposition.

The polytype behavior observed here for BCM is consistent with behavior observed in the parent perovskite BMO, which also shows polytypes with increasing oxygen non-stoichiometry.⁴¹ The phase changes in BMO are related to distortions caused by different ordering of octahedral layers. As first shown by Matias et al.^{39,40}, the polytypes for 12R and 10H also include cerium cation ordering. This makes the phase transitions relatively slow. STCH WS cycle tests are insufficient in duration (~ 5 minutes) to permit the 12R to 10H phase change; the 10H phase can only be obtained when reducing the BCM material at higher temperatures for long times (several hours). We produced a pure 10H sample and did simulated WS cycles in the TGA with O₂ flow instead of steam (results shown in the SI). After several redox runs, the 10H sample converted fully to 12R phase (demonstrated by the XRD) and subsequently remained in the 12R phase. The detailed thermodynamics of this system and its various polytypes is the subject of ongoing study. The intriguing nature of these distortional-type phase changes, which do not coincide with full changes in oxygen stoichiometry, (like those of early STCH materials like FeO to Fe₂O₃^{1,42}) points towards a potentially exciting new mechanism for enhancing the per-cycle hydrogen productivity in BCM and related STCH-active perovskite systems.

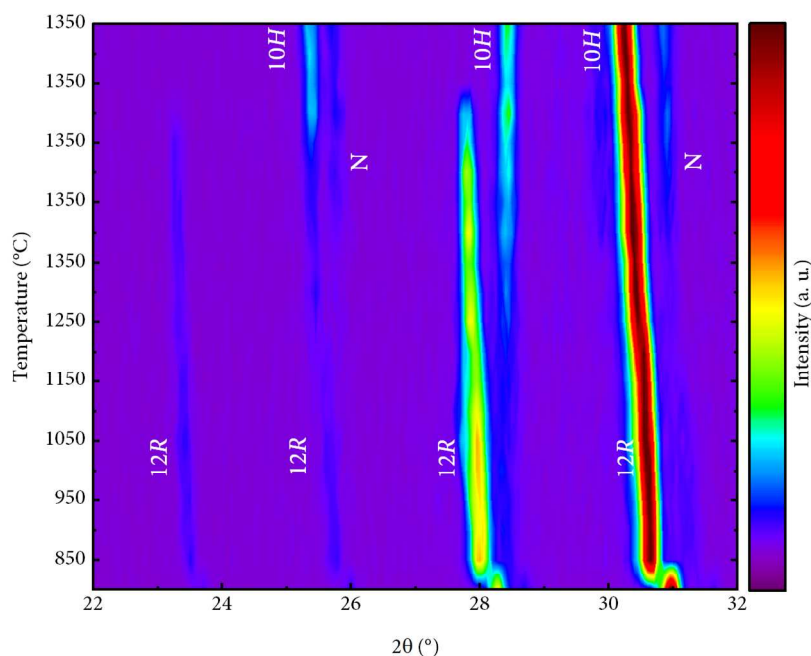


Figure 2 – High Temperature XRD done on a 12R-BaCe_{0.25}Mn_{0.75}O_{3-δ} sample, heating from room temperature to 1350 °C in He flow. At 1150 °C the 12R phase starts to convert to 10H phase and by 1350 °C the onset of a new H polytype phase (N) is also apparent.

The samples were subjected to our Temperature Programmed Reduction screening protocol in order to quantify their redox behavior in comparison to previously identified STCH candidates (ceria, SLMA4664 and SLMA6464), as shown in Figure 3. SLMA4664 and SLMA6464 are used for comparison here because they are perovskite oxides with promising water splitting capacity,^{24,37} despite showing very strong kinetic limitations, while ceria (a fluorite) is the current benchmark material for STCH application.⁶ Ceria and SLMA6464 essentially represent boundaries of the STCH performance space of interest. Ceria provides an upper boundary with its unmatched reoxidation capability but low extent of reduction, while SLMA6464 provides a lower boundary due to its large extent of reduction but poor reoxidation performance. From a cycle thermodynamic perspective, any promising material will likely need to fall in between these two limits.⁹

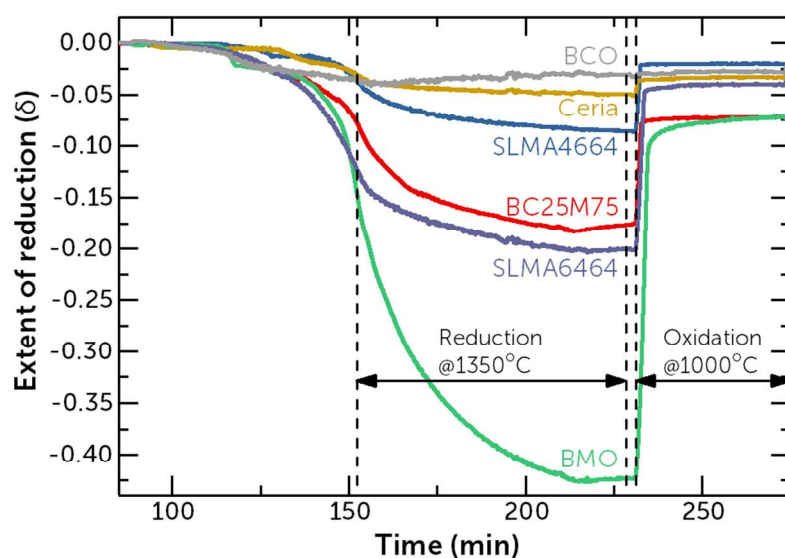


Figure 3 – Temperature Programmed Reduction experiment evaluates the extent of reduction (formation of oxygen vacancies or δ) and reversibility of samples BCO, ceria, SLMA 4664, BC25M75, SLMA6464 and BMO. Reduction at 1350 °C for 1 h and Oxidation in air at 1000 °C.

The TPR experiment reveals that BCO has no significant reduction and poor reoxidation for the water splitting application. BMO, on the other hand, reduces to an extreme (i.e., to a far greater extent than even BCM), which indicates that the driving force for reoxidation will likely be too low to split water. These TPR results are consistent with the E_v and oxygen bond strength estimates for BMO and BCO provided in Table 1.

As viable STCH materials must be cycle-able, mass recovery upon reoxidation is also an important consideration. While it should be noted that none of the experiments in Figure 3 show a

complete return to zero upon oxidation, that is not necessarily indicative of whether samples experienced complete reoxidation. Testing is conducted on as-calcined powders with only a low temperature burnout (500 °C in air) before the experiment. While this removes most sources of irreversible mass loss, e.g., largely surface adsorbed water and stray organics, some irreversible mass losses not related to reduction may still occur upon heating to 1350 °C (e.g., strongly bound water, residual surface carbonates and hydroxides, etc.). As a general guideline, we typically consider materials that reoxidize to within a net difference in oxygen non-stoichiometry ($\Delta\delta$) of < 0.05 (representing a recovery to within $\sim 0.2\%$ of the starting mass) to be fully reoxidized, and therefore reversible/cycle-able.

BMO did not return to its original stoichiometry after reoxidation, which may indicate stability issues such as sintering and/or partial decomposition. BC25M75 also failed to completely reoxidize during initial testing, however, on subsequent cycling, no further unrecoverable reduction occurred (as shown in Figure S4).

The water splitting capability of six materials; BMO, BC25M75, BC50M50, BC75M25, BCO, and ceria (used as a reference) were tested at the SFR under the reduction condition of T_{RE} 1350 °C and oxidation condition of T_{OX} 1000 °C with 40 vol. % of H₂O. H₂ production was highest for the BC25M75 composition, falling off sharply for compositions on either side. Neither end-member composition (BCO, BMO) splits water under the test conditions used. Based on the prior TPR results, we conjecture that BCO does not sufficiently reduce at $T_{RE} = 1350$ °C, and therefore does not split a detectable amount of water upon exposure to steam in the reoxidation step at 1000 °C. In contrast, BMO reduces too easily, and therefore likely does not provide sufficient driving force for water splitting upon exposure to steam at T_{OX} 1000°C. As shown in Figure 4, the average H₂ production for the intermediate compositions (BC25M75, BC50M50, and BC75M25) closely correlates with the amount of $12R\text{-BaCe}_{0.25}\text{Mn}_{0.75}\text{O}_{3-\delta}$ phase present in each sample. Early on, we therefore concluded that the $12R\text{-BaCe}_{0.25}\text{Mn}_{0.75}\text{O}_{3-\delta}$ phase represents the dominant active water splitting compound in this compositional family. Only later, as discussed above, did it become apparent that the distinction between the 10H and 12R was unnecessary for this analysis.

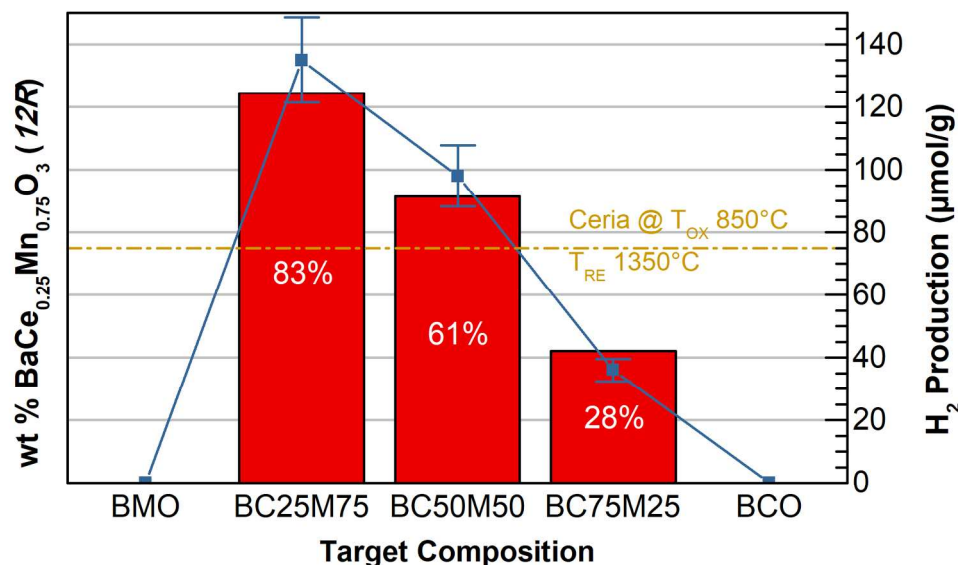


Figure 4 – Average H_2 productivity over 3 cycles ($\mu\text{mol H}_2/\text{g}$ sample) for BMO, BC25M75, BC50M50, BC75M25, BCO, and ceria (included as a reference). Superimposed on this data is the relative phase fraction of the hypothesized active water-splitting phase ($12R\text{-BaCe}_{0.25}\text{Mn}_{0.75}\text{O}_{3-\delta}$) in each sample. H_2 productivity closely correlates with the percentage of $12R\text{-BaCe}_{0.25}\text{Mn}_{0.75}\text{O}_{3-\delta}$ present in each sample.

It is important to note that the BC25M75 and BC50M50 samples contain small amounts (less than 5 %) of ceria as a secondary phase, and ceria is clearly an active WS material. Scaling the H_2 productivity of ceria by the percentage of ceria phase present in these samples, however, suggests that ceria is responsible for only a small portion of the total WS response of these materials under the applied test conditions. In BC25M75 and BC50M50, for example, the residual ceria should contribute less than $\sim 1 \mu\text{mol/g}$ to the H_2 production, far smaller than the $135 \mu\text{mol/g}$ and $97 \mu\text{mol/g}$ of total H_2 production measured for these samples respectively. Even for BC75M25, which contains $\sim 15\%$ ceria, only $\sim 5 \mu\text{mol/g}$ of H_2 can be attributed to the ceria phase, with the rest of the $\sim 40 \mu\text{mol/g}$ of total H_2 production attributable to the $12R\text{-BaCe}_{0.25}\text{Mn}_{0.75}\text{O}_{3-\delta}$ phase. This analysis supports our supposition that $\text{BaCe}_{0.25}\text{Mn}_{0.75}\text{O}_{3-\delta}$ is the dominant water splitting phase in these samples under the applied test conditions. Subsequently, pure phase $12R\text{-BaCe}_{0.25}\text{Mn}_{0.75}\text{O}_{3-\delta}$ (which for simplicity we abbreviate as BCM hereinafter) was synthesized and became the primary material for continued investigations.

BCM was tested for water splitting at $T_{\text{RE}} 1350^\circ\text{C}$ for 330 s and $T_{\text{OX}} 850^\circ\text{C}$ with 40 vol% H_2O for 1200 s and compared to ceria (the benchmark STCH material) and SLMA4664 (currently the most promising STCH perovskite) under the same experimental conditions using the same testing protocol.

Representative water splitting cycle data for BCM, SLMA4664, and ceria are shown in Figure 5. Each sample was subjected to an initial reduction step from a fully oxidized state followed by two complete water splitting cycles, each comprised of a reoxidation step and a subsequent reduction step.

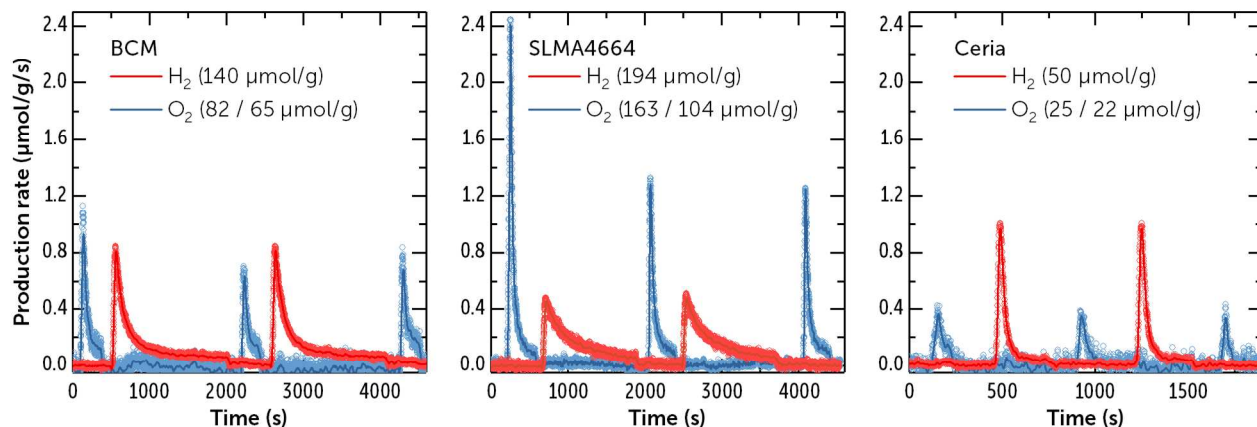


Figure 5 - Water splitting experiment at T_{RE} 1350 °C for 330 s and T_{OX} 850 °C with 40 vol% H₂O for 1200 s. Ceria was oxidized for 300 s. O₂ peaks (blue) and H₂ peaks (red) record the amount of oxygen and hydrogen evolved per gram of sample as a function of time. Integrated totals for the first three peaks are listed in the legend.

While SLMA4664 releases a much larger amount of O₂ during the initial reduction than the other materials, significantly less O₂ (~60-70% of the initial cycle amount) is released during subsequent reduction cycles. This is because the water splitting step is strongly kinetically and thermodynamically limited in SLMA. SLMA4664 is unable to fully reoxidize during the allotted cycle time, which was chosen to approximate cycle times associated with a commercial water splitting reactor that does not incorporate material storage. BCM shows a similar, but far less severe kinetic limitation, as the O₂ evolved during the initial reduction step is slightly greater than that evolved in subsequent reduction cycles. Ceria, in contrast, evolves the same amount of O₂ in the initial reduction and in subsequent reduction cycles, indicating that its WS kinetics are sufficiently fast to permit full reoxidation within the experimental cycle time.

In order to quantitatively compare the water splitting kinetics of BCM, SLMA4664, and ceria, all three were evaluated using a simplified solid-state kinetics model, the details of which are briefly described in the Supplemental Information. The second-order “F2” kinetic model has been shown to produce a good fit for ceria, and we find that it can also nicely fit the BCM kinetic behavior. We therefore applied this model to analyze all three materials. The broad SLMA4664 H₂ peak shape (as shown in Figure 5b), suggests a strong transport limitation and therefore doesn’t provide a good fit using only F2. As reported previously,^{24,37} SLMA4664 requires a coupled kinetic model where first-order reaction and

diffusion are considered in concert. While such analysis is outside the scope of the present study, this observation further reinforces the fact that SLMA4664 presents additional kinetic limitations compared to BCM and ceria. Table 2 summarizes the rate constants (k_o) determined for ceria, BCM, and SLMA4664 fit to the F2 model at T_{RE} 1350 °C and T_{OX} 850 °C and 1000 °C, respectively.

Table 2 – Summary of the oxidation reaction rate constants using the second-order kinetics model F2 for BCM and Ceria at T_{OX} 850 °C and 1000 °C.

T_{OX} (°C)	Sample	$r_{H_2} \propto k_o Y_{H_2O} (1 - \alpha)^2$ [s ⁻¹]		
		k_o [s ⁻¹]		log k_o
		H ₂ peaks average	Standard deviation	
850	SLMA4664	0.0075	0.0005	-2.12
	BCM	0.0131	0.0005	-1.88
	CeO ₂	0.1827	0.0189	-0.74
1000	SLMA4664	0.0078	0.0005	-2.11
	BCM	0.0161	0.0005	-1.79
	CeO ₂	0.0756	0.0015	-1.12

It is worth noticing that the calculated rate constants for BCM increase with the increase in T_{OX} , whereas for ceria k_o decreases about 2.5 times with the increase in temperature. This indicates that ceria's reaction kinetics are slower at the 1000 °C compared to 850 °C. SLMA's reoxidation kinetics are the slowest of all three materials. This behavior is further evident when analyzing Figure 6. In this plot, the as-measured mass normalized H₂ production rate for each material (scattered dots) is compared against the kinetic model (solid lines). Time is plotted in logarithmic scale for better visualization of the plot features.

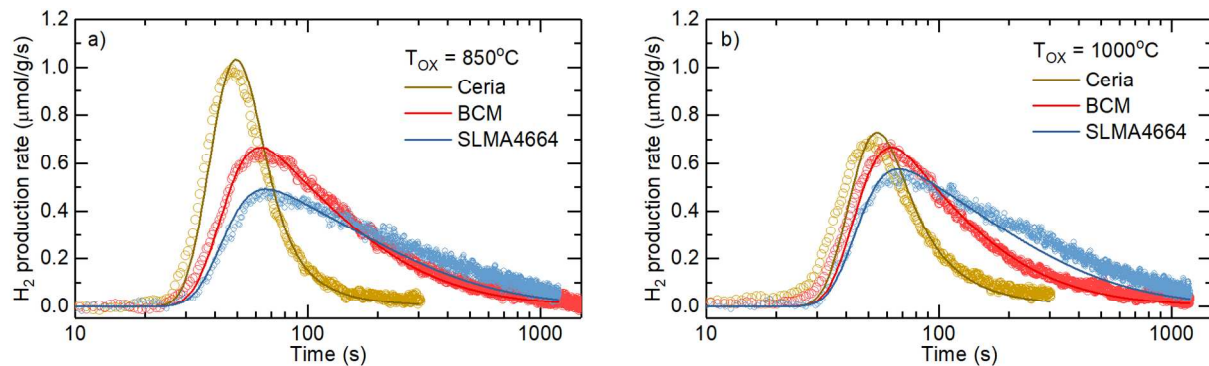


Figure 6 – Mass normalized H_2 production rate as a function of time (scattered dots) measured during WS at T_{RE} 1350 °C and T_{OX} (a) 850 °C and (b) 1000 °C at 40 vol. % steam, and best fit (solid lines) derived from the solid-state kinetic model assuming second-order reaction. More details described in the SI.

To further evaluate and compare BCM's hydrogen production capacity against our implied standards, all three materials were examined under a range of oxidation and reduction conditions; namely variable T_{OX} and oxidizing potential of the argon-steam mixture. Figure 7 summarizes the total amount of H_2 produced by ceria, BCM, and SLMA4664 during STCH cycling in the SFR with 40% steam, $T_{RE} = 1350$ °C, and $T_{OX} = 750, 850,$ and 1000 °C, respectively. The BCM, SLMA4664, and ceria hydrogen production data for two other reduction temperatures is compiled in Table S4 of the Supporting Information. Ceria's net hydrogen capacity is essentially independent of oxidation temperature for the conditions investigated. On the other hand, the positive slopes for BCM and SLMA4664 demonstrate that their oxidation kinetic limitations can be countered, to an extent, by increasing the oxidation temperature. SLMA4664, in particular, benefits greatly by the 150 °C increase from 850 °C to 1000 °C and shows larger H_2 productivity than ceria and BCM over all the temperatures tested. In considering a comparative analysis between these STCH materials, it should be noted that H_2 yield is highly sensitive to absolute cycle times making direct comparisons to previous works uninformative.²⁴

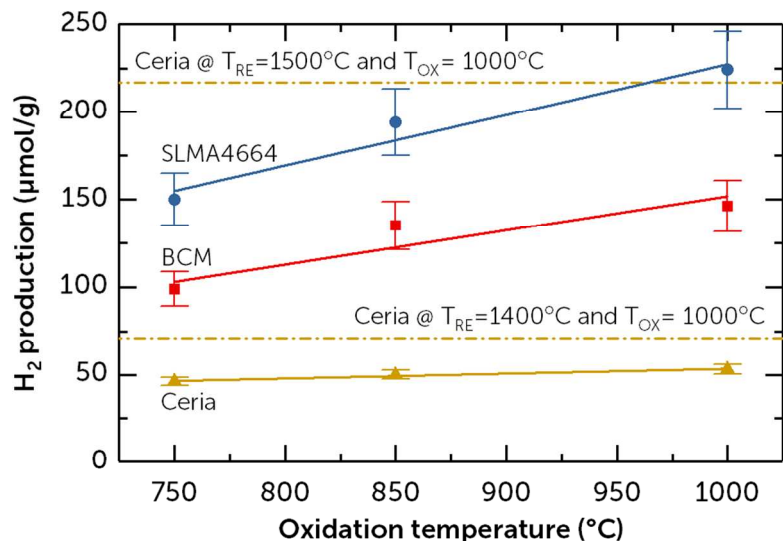


Figure 7 – Total H_2 produced per cycle by BCM (square), SLMA4664 (circle) and ceria (triangle) at T_{RE} of 1350 °C with 40 vol. % steam and various oxidation temperatures. Reduction heating rate is 10 °C/s, with a reduction time of 330 s and a reoxidation time of 1200 s.

Materials that support STCH cycle operation at lower T_{RE} and T_{OX} are greatly desired for practical reactor applications as this relaxes high-temperature reactor materials requirements and generally improves overall reactor efficiency, due to decreased thermal losses and less energy required to heat both redox material and steam. From this perspective, SLMA4664 appears highly attractive as it yields significantly more H_2 than either ceria or BCM across a range of T_{RE} and T_{OX} conditions, and particularly at lower T_{RE} and T_{OX} (see Figures S5a and S5b in the Supporting Information). BCM (at T_{RE} 1350 °C and T_{OX} 1000 °C) does approach ceria's high-temperature performance window by 2/3 (at T_{RE} 1500 °C and $T_{\text{OX}} = 1000$ °C),³⁷ but at a substantially lower cycle ΔT . However, BCM yields less H_2 than SLMA4664 at all temperatures placing its performance characteristics in between our two material endpoint standards when a relatively high oxidizing potential of the argon-steam mixture is used to drive the reoxidation reaction to near completion.

In addition to CeO_2 and SLMA, a number of other oxides have been studied for potential STCH application; a summary of these alternative materials is provided in Table S5 of the SI for reference. These materials have generally been tested at higher reduction temperatures (T_{RE} 1400-1500 °C) and larger steam concentrations than we used in our experiments, making a direct comparison vs. BCM difficult. More crucially, however, most of these alternative systems require significantly longer reduction and oxidation cycle times (from 30 minutes to 5 hours), due to kinetic limitations associated with the redox process. For example, several of the transition-metal doped cerates and poly-cation oxides summarized in Table S5 show higher *per-cycle* H_2 yields than BCM, but when taking into account the length of the redox cycle they show lower H_2 productivity *per unit time on sun* than BCM.

In addition to fast redox kinetics, viable STCH materials must also be able to split water under “high conversion” conditions, where the ratio of $\text{H}_2\text{O}:\text{H}_2$ needed to drive the cycle to completion is substantially below 1000:1 (and ideally less than 10:1⁹). This is of extreme importance because the solar-to-hydrogen conversion efficiency and commercial viability of STCH production technology are tightly coupled to the process steam requirement.⁹ Unfortunately, most candidate STCH materials have only been studied under conditions that approach the “zero conversion” limit (e.g., steam in argon) where the $\text{H}_2\text{O}:\text{H}_2$ is undefined, but certainly $\gg 10,000:1$.

In order to examine the performance of candidate materials under high conversion conditions, we supplied a mixture of H_2 and argon to the 40 % steam (rather than balancing the 40 % steam with inert gas only) during the water splitting step to establish well-defined $\text{H}_2\text{O}:\text{H}_2$ ratios. We tested ceria, SLMA4664, and BCM with steam-to-hydrogen ratios of 1333:1, 1000:1, 750:1, 500:1 and 285:1 using T_{RE} 1350 °C and T_{OX} 850 °C as thermal conditions for the cycle. The results are presented in Figure 8.

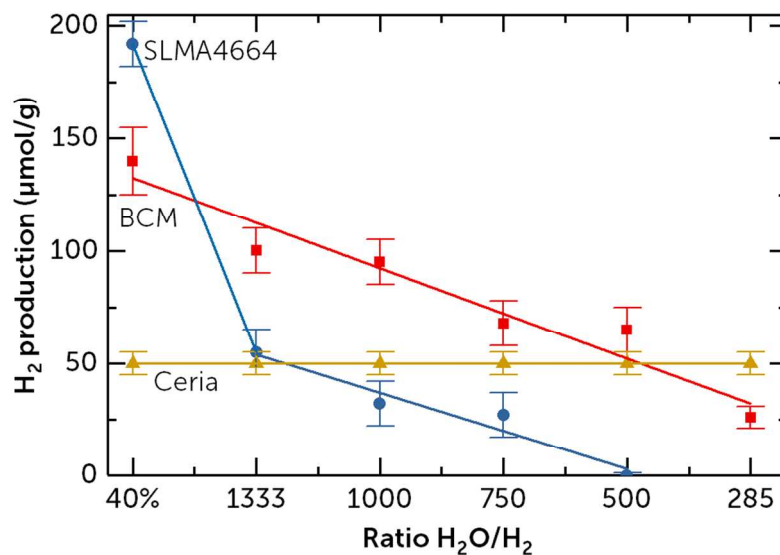


Figure 8 – “High conversion” water splitting performed at various steam to hydrogen mixture ratios for all three materials: BCM (square), SLMA4664 (circle), and ceria (triangle) at T_{RE} 1350 °C and T_{OX} 850 °C.

Ceria’s net hydrogen production capacity is unchanged when the initial oxidizing potential of the WS gas mixture is held at equivalent O_2 partial pressures between 2.5×10^{-12} (1333:1) and 1.0×10^{-13} (285:1) atmospheres. This insensitivity to low $H_2O:H_2$ ratios is due in part to the high oxygen vacancy formation energy found in ceria, which provides a strong thermodynamic driving force for water splitting even under strongly reducing conditions. SLMA4664 on the other hand, sharply deactivates in the presence of residual hydrogen (water splitting no longer proceeds at $H_2O:H_2$ ratios of 500:1). Thus, although SLMA4664 is promising due to its high extent of reduction and large H_2 production capacity under abundance of steam, the economics of using SLMA in practical water splitting reactors is severely challenged because of low WS favorability under realistic $H_2O:H_2$ ratios desired for efficient reactor operation.²⁵ BCM, on the other hand, shows promising tolerance to high conversion conditions. While water splitting capacity in BCM gradually falls off as the $H_2O:H_2$ ratio decreases, it does not suffer from the drastic drop in performance seen in SLMA, and it maintains H_2 production close to that of ceria down to the 285:1 $H_2O:H_2$ ratio. This is the first known perovskite-based oxide to demonstrate acceptable performance under high conversion conditions. Recently Zhai et al.⁴³ showed that the poly-cation oxide $(FeMgCoNi)O_x$ also has the ability to split water under similar high conversion conditions (1000:1 $H_2O:H_2$) under similar temperature swing limits of T_{RE} 1300 °C and T_{OX} 800 °C explored in the work. This material showed promising performance yielding more H_2 than ceria at that ratio and showing a similar trend to BCM, with a decrease in H_2 yield with an increase in conversion ratio to about 100:1,

however at the cost of long reduction and oxidation cycles of 5 h each. Within the same time frame of 10 hours, BCM would surpass their H_2 production for all steam-to-hydrogen ratios lower than about 300:1.

Structural and compositional durability is an additional concern for any proposed redox active material because of the extreme chemical and thermal stresses encountered in a STCH cycle. Limited lifetime testing has been performed on BCM through rapid redox cycling (210 s reduction and 10 min oxidation) in the SFR showing no deterioration in performance over 50 water-splitting cycles (ΔT between T_{RE} 1350 °C and T_{OX} 850 °C) under 40 vol. % steam as shown in Figure 9. It is worth noting that the scattering in the integrated hydrogen peaks for each cycle shown in Figure 9b, is due to variations in the mass spectrometer detection.

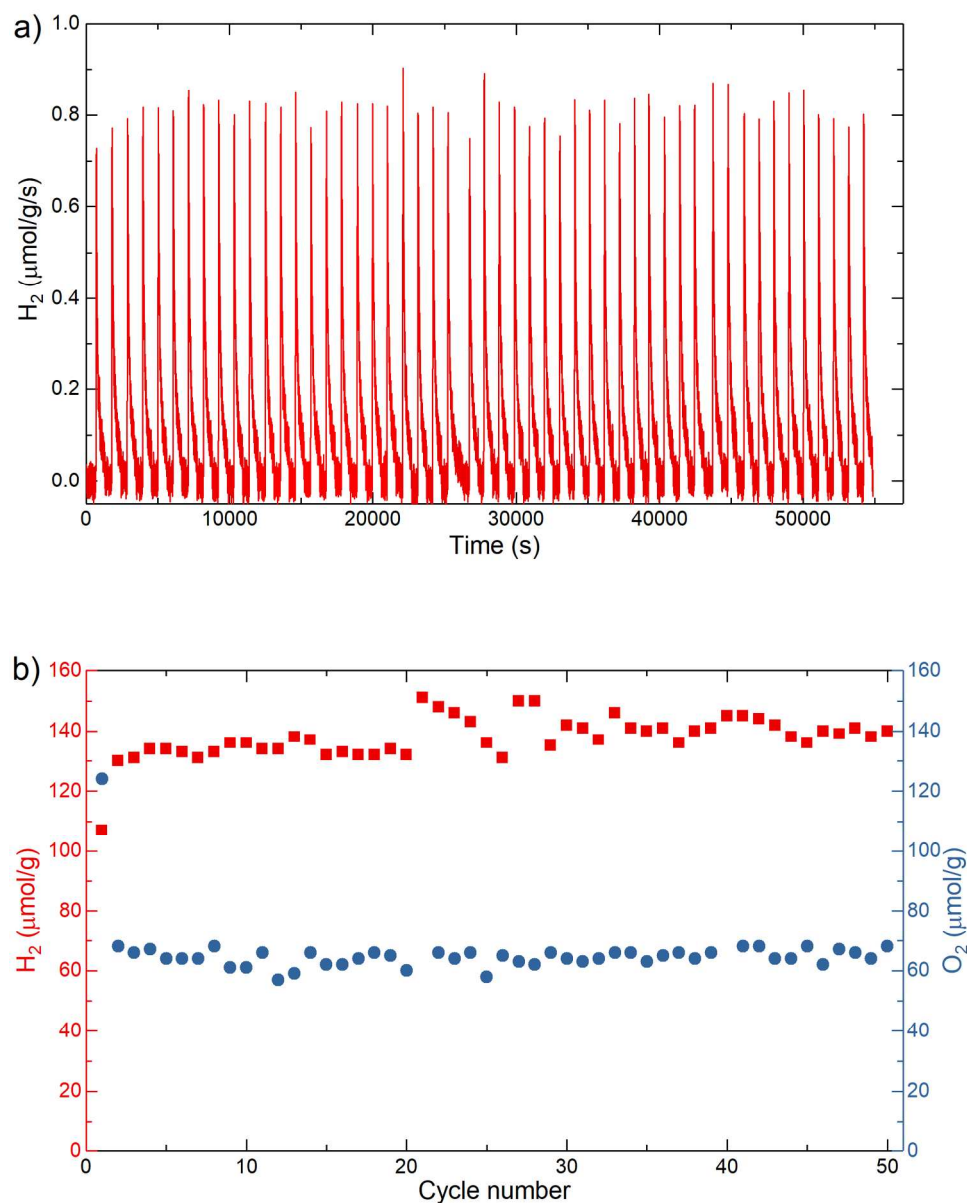


Figure 9 – Stability experiment done in the BCM sample. The fifty hydrogen peaks are shown in (a) and the integrated amounts of O₂ and H₂ obtained in each cycle are plotted in (b). Reduction was done at T_{RE} 1350 °C for 210 s and oxidation with 40 vol. % steam was carried out at T_{OX} 850 °C for 10 min. The data was collected over three days of experiment.

While it is believed that the 12R/10H phase change does not have sufficient time to occur during rapid STCH cycling, this preliminary lifetime testing suggests that even if the phase change does occur, it is clearly not detrimental to the water splitting performance. Post-mortem XRD performed after the 50 cycles experiment reveals only the presence of the 12R phase. This is a promising result because poor durability and phase instability have hampered other prospective STCH redox materials systems.^{13,44} We speculate that if the conditions were altered such that the phase change could occur during cycling, the phase change thermodynamics could in fact boost the WS performance. The molar volume per formula unit of 12R is slightly lower than that of the 10H phase, suggesting a slight increase in the standard absolute entropy of the system upon phase conversion⁴⁵. If this phenomenon could be successfully exploited, it would represent the first example of a perovskite where nonstoichiometry participates in both phases during reaction.

CONCLUSION

The search for viable STCH materials within the vast perovskite oxide space has led to the discovery of a potentially attractive alternative to ceria, BaCe_{0.25}Mn_{0.75}O₃. With greatly improved reduction capacity at temperatures < 1400 °C, BCM produces 140 μmol/g of hydrogen at T_{RE} = 1350 °C and T_{OX} = 850 °C, nearly a three-fold improvement over ceria at these same conditions. And while BCM does not ultimately have the large production capacity exhibited by another notable Mn-based candidate perovskite (Sr_{0.4}La_{0.6}Mn_{0.6}Al_{0.4}O₃) under oxidation in excess steam, it does have distinctively faster reoxidation kinetics and greatly improved tolerance to the presence of hydrogen in the oxidation half cycle. In fact, BCM is the first example of a perovskite demonstrated to retain water splitting capability under high conversion conditions (steam-to-hydrogen ratio in the order of 285:1). This combination points to the potential of much higher overall solar-to-hydrogen conversion efficiencies than previous solar thermochemical water splitting candidates based on nonstoichiometry in perovskite or fluorite crystal structures.

Perhaps more important than BCM's performance is its novel combination of properties that opens new paths towards STCH materials discovery. The presence of cerium on the B-site of the

perovskite and its positive contribution to water-splitting opens the possibility of further focused search for other candidate materials that can accommodate the addition of cerium as a major dopant, while the intriguing prospect of leveraging polytypes with different thermodynamics and oxygen non-stoichiometry creates further new avenues for investigation.

ACKNOWLEDGEMENTS

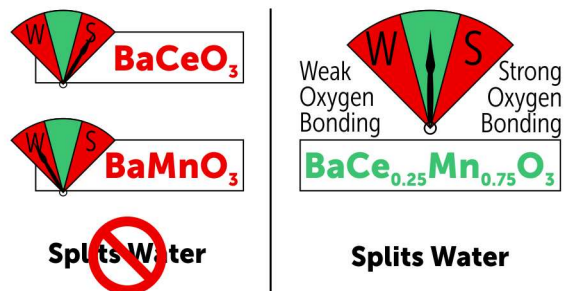
The authors gratefully acknowledge research support from the HydroGEN Advanced Water Splitting Materials Consortium, established as part of the Energy Materials Network under the U.S. Department of Energy, Office of Energy Efficiency and Renewable Energy, Fuel Cell Technologies Office, under Award Number DE-EE0008087. Sandia National Laboratories is a multimission laboratory managed and operated by National Technology and Engineering Solutions of Sandia LLC, a wholly owned subsidiary of Honeywell International Inc., for the U.S. Department of Energy's National Nuclear Security Administration under contract DE-NA0003525. We would also like to acknowledge Dr. Eric Coker for the HTXRD experiment contribution. These experiments were carried out at Sandia National Laboratories Albuquerque. We finally acknowledge the financial support (scholarship process number BEX: 13452-13-4) provided by CAPES (Coordination for the Improvement of Higher Education Personnel) and the Science Without Borders Program granted by the Brazilian government.

REFERENCES

- 1 T. Nakamura, *Sol. Energy*, 1977, **19**, 467–475.
- 2 R. Perret, *Solar thermochemical hydrogen production research (STCH): Thermochemical cycle selection and investment priority*, 2011.
- 3 S. Abanades, P. Charvin, G. Flamant and P. Neveu, *Energy*, 2006, **31**, 2805–2822.
- 4 T. Kodama and N. Gokon, *Chem. Rev.*, 2007, **107**, 4048–4077.
- 5 M. D. Allendorf, R. B. Diver, N. P. Siegel and J. E. Miller, *Energy & Fuels*, 2008, **22**, 4115–4125.
- 6 W. C. Chueh, C. Falter, M. Abbott, D. Scipio, P. Furler, S. M. Haile and A. Steinfeld, *Science*, 2010, **330**, 1797–1801.
- 7 W. C. Chueh and S. M. Haile, *ChemSusChem*, 2009, **2**, 735–739.
- 8 W. C. Chueh and S. M. Haile, *Philos. Trans. A. Math. Phys. Eng. Sci.*, 2010, **368**, 3269–3294.
- 9 A. H. McDaniel, *Curr. Opin. Green Sustain. Chem.*, 2017, **4**, 37–43.
- 10 I. Ermanoski, J. E. Miller and M. D. Allendorf, *Phys. Chem. Chem. Phys.*, 2014, **16**, 8418–8427.
- 11 N. P. Siegel, J. E. Miller, I. Ermanoski, R. B. Diver and E. B. Stechel, *Ind. Eng. Chem. Res.*, 2013, **52**, 3276–3286.
- 12 E. A. Fletcher and R. L. Moen, *Science (80-.)*, 1977, **197**, 1050–1056.
- 13 J. E. Miller, A. H. McDaniel and M. D. Allendorf, *Adv. Energy Mater.*, 2014, **4**, 1–19.
- 14 J. R. Scheffe and A. Steinfeld, *Energy & Fuels*, 2012, **26**, 1928–1936.
- 15 Y. Hao, C.-K. Yang and S. M. Haile, *Chem. Mater.*, 2014, **26**, 6073–6082.

- 16 N. Gokon, T. Suda and T. Kodama, *Thermochim. Acta*, 2015, **617**, 179–190.
- 17 Q. Jiang, G. Zhou, Z. Jiang and C. Li, *Sol. Energy*, 2014, **99**, 55–66.
- 18 J. R. Scheffe, R. Jacot, G. R. Patzke and A. Steinfeld, *J. Phys. Chem. C*, 2013, **117**, 24104–24114.
- 19 T. I. Qing-Long Meng, Chong-il Lee and Y. T. Hiroshi Kanekob, *Int. J. Hydrogen Energy*, 2011, **36**, 13435–13441.
- 20 M. Kubicek, A. H. Bork and J. L. M. Rupp, *J. Mater. Chem. A*, 2017, **5**, 11983–12000.
- 21 A. Jun, J. Kim, J. Shin and G. Kim, *ChemElectroChem*, 2016, **3**, 511–530.
- 22 M. Luo, Y. Yi, S. Wang, Z. Wang, M. Du, J. Pan and Q. Wang, *Renew. Sustain. Energy Rev.*, 2018, **81**, 3186–3214.
- 23 A. Vojvodic and J. K. Nørskov, *Science*, 2011, **334**, 1355–1356.
- 24 A. H. McDaniel, E. C. Miller, D. Arifin, A. Ambrosini, E. N. Coker, R. O’Hayre, W. C. Chueh and J. Tong, *Energy Environ. Sci.*, 2013, **6**, 2424.
- 25 M. Takacs, M. Hoes, M. Caduff, T. Cooper, J. R. Scheffe and A. Steinfeld, *Acta Mater.*, 2016, **103**, 700–710.
- 26 A. M. Deml, A. M. Holder, R. P. O’Hayre, C. B. Musgrave, V. Stevanovic, R. P. O. Hayre, C. B. Musgrave and V. Stevanović, *J. Phys. Chem. Lett.*, 2015, **18**, 1948–1953.
- 27 S. S. Naghavi, A. A. Emery, H. A. Hansen, F. Zhou, V. Ozolins and C. Wolverton, *Nat. Commun.*, 2017, **8**, 285.
- 28 S. Lany, *J. Chem. Phys. J. Chem. Phys. J. Chem. Phys. J. Chem. Phys.*, 2018, **148**, 71101–81101.
- 29 C.-K. Yang, Y. Yamazaki, A. Aydin and S. M. Haile, *J. Mater. Chem. A*, 2014, **2**, 13612–13623.
- 30 Y. Luo and J. Kerr, *CRC Handb. Chem. Phys.*, 2007, 65–98.
- 31 M. Ezbiri, K. M. Allen, M. E. G??lvez, R. Michalsky and A. Steinfeld, *ChemSusChem*, 2015, **8**, 1966–1971.
- 32 R. Glöckner, M. S. Islam and T. Norby, *Solid State Ionics*, 1999, **122**, 145–156.
- 33 M. Shang, J. Tong and R. O’Hayre, *Mater. Lett.*, 2013, **92**, 382–385.
- 34 J. R. Scheffe, M. D. Allendorf, E. N. Coker, B. W. Jacobs, A. H. McDaniel and A. W. Weimer, *Chem. Mater.*, 2011, **23**, 2030–2038.
- 35 J. R. Scheffe, A. H. A. H. McDaniel, M. D. Allendorf and A. W. Weimer, *Energy Environ. Sci.*, 2013, **6**, 963–973.
- 36 D. Arifin, V. J. Aston, X. Liang, A. H. McDaniel and A. W. Weimer, *Energy Environ. Sci.*, 2012, **5**, 9438–9443.
- 37 A. H. McDaniel, A. Ambrosini, E. N. Coker, J. E. Miller, W. C. Chueh, R. O’Hayre and J. Tong, *Energy Procedia*, 2013, **49**, 2009–2018.
- 38 A. F. Fuentes, K. Boulahya and U. Amador, *J. Solid State Chem.*, 2004, **177**, 714–720.

- 39 M. A. Macías, O. Mentre, S. Colis, G. J. Cuello and G. H. Gauthier, *J. Solid State Chem.*, 2013, **198**, 186–191.
- 40 M. A. Macías, O. Mentré, C. Pirovano, P. Roussel, S. Colis and G. H. Gauthier, *New J. Chem.*, 2015, **39**, 829–835.
- 41 J. J. Adkin and M. A. Hayward, , DOI:10.1021/cm062055r.
- 42 C. L. Muhich, B. D. Ehrhart, I. Al-Shankiti, B. J. Ward, C. B. Musgrave and A. W. Weimer, *Wiley Interdiscip. Rev. Energy Environ.*, 2015, **5**, 261–287.
- 43 S. Zhai, J. Rojas, N. Ahlborg, K. Lim, M. Toney, H. Jin, W. C. Chueh and A. Majumdar, *Energy Environ. Sci.*, , DOI:10.1039/c8ee00050f.
- 44 T. Kodama, N. Gokon and R. Yamamoto, *Sol. Energy*, 2008, **82**, 73–79.
- 45 H. Donald, B. Jenkins and L. Glasser, *Inorg. Chem.*, 2003, **42**, 8702–8708.



BCM is a new water-splitting STCH material with promising high-conversion performance and kinetics, formed from two non water-splitting parent perovskites.

TOC Statement (20 words):

BCM is a new water-splitting STCH material with promising high-conversion performance and kinetics, formed from two non water-splitting parent perovskites.

Broader Context Statement (200 words):

The conversion of solar energy to usable and storable chemical energy (typically in a convenient fuel) continues to be at the fore-front of renewable energy research. One intriguing process for efficiently generating industrial-scale quantities of hydrogen from full-spectrum sunlight is Solar Thermochemical Hydrogen (STCH) production -- the conversion of concentrated solar power directly into hydrogen via high-temperature two-step thermochemistry. Despite previous advances in using perovskite-structure oxides, the necessary process targets for STCH materials remain out of reach. Attempts to improve hydrogen production capacity, normally by improving the ease of oxide reduction, generally lead to a loss of thermochemical water-splitting activity due to inherent thermodynamic tradeoffs. This loss affects the material's ability to continue to split water in the presence of hydrogen. BCM is a first of its kind perovskite oxide that improves on some of the limitations of the previous perovskites, sacrificing a small amount of capacity for greatly improved hydrogen production under low pO₂ conditions. The novel structure also opens new avenues for further improvement and informs the search for additional potential STCH compounds.